Experimental determinations of Flame Describing Functions of swirling spray flames

Kevin Prieur, Daniel Durox, Guillaume Vignat, Thierry Schuller, Sébastien Candel

Colloque INCA, 18-19/10/2017
Safran Paris Saclay, Rue des jeunes Bois, 78117 Châteaufort

Experimental determinations of Flame Describing Functions of swirling spray flames

Kevin Prieur · Daniel Durox · Guillaume Vignat · Thierry Schuller · Sébastien Candel

Abstract Studies of the dynamics of spray swirling flames are of importance from a fundamental point of view and also because these flames are used in many practical systems like aero-engine combustors. Under certain conditions these flames give rise to various types of undesirable combustion instabilities. This article focuses on the measurement of the combustion dynamics of a system comprising a single injector designated as SICCA-Spray and reports novel Flame Describing Function (FDF) data on spray swirling flames. The test configuration comprises a tubular plenum fed with air by a swirling injector, a simplex atomizer that injects the liquid fuel (n-heptane) within a hollow cone spray and a cylindrical combustion chamber where the air and the fuel spray mix and burn. The air flow can be excited with two driver units plugged on the plenum, creating a flow perturbation which acts on the flame. The amplitude of fluctuation u' is controlled with a hot wire in the plenum. The flame response to incoming perturbations is then examined by recording the OH* signal with a photomultiplier equipped with an interferometric filter. It is assumed that fluctuations of the light emission from this excited radical is proportional to heat release rate perturbations $\dot{Q}'$. The acoustic pressure p' at the backplane of the chamber is also recorded with a cooled waveguide microphone. Two different FDFs are defined and compared: $\dot{Q}'/\overline{\dot{Q}} = f\,(p'/\bar{p})$ and $\dot{Q}'/\overline{\dot{Q}} = g\,(u'/\bar{u})$. The data are then used to analyze self-excited instabilities observed in the SICCA-Spray burner and to interpret some recent observations of strong self-sustained azimuthal instabilities in the MICCA-Spray annular combustor, equipped with sixteen injectors identical to that used in the SICCA-Spray set-up.

Keywords Combustion dynamics · Flame Transfer Function · Flame Describing Function · Spray flames

1 Introduction

Advanced combustion systems developed for aircraft engines may give rise to combustion instabilities. These instabilities are one of the major problems encountered in the design of the new generation of low-emission modern engines. Since most practical combustors in aero-engines or in gas turbines feature an annular geometry an increasing number of investigations has been devoted to the analysis of thermoacoustic coupling in such configurations [1–7]. There are yet very few

Kevin Prieur
Safran Tech, E&P, Châteaufort, CS 80112, 78772 Magny-Les-Hameaux, France
Laboratoire EM2C, CNRS, CentraleSupélec, Université Paris-Saclay, 3, rue Joliot Curie, 91192 Gif-sur-Yvette cedex, France
E-mail: kevin.prieur@centralesupelec.fr

Guillaume Vignat, Daniel Durox, Sébastien Candel
Laboratoire EM2C, CNRS, CentraleSupélec, Université Paris-Saclay, 91190 Gif-sur-Yvette cedex, France

Thierry Schuller Laboratoire EM2C, CNRS, CentraleSupélec, Université Paris-Saclay, 91190 Gif-sur-Yvette cedex, France
Institut de Mécanique des Fluides de Toulouse (IMFT), Université de Toulouse, CNRS, INPT, UPS, Toulouse, France

works reported on annular systems powered by liquid fuels ,with the exception of LES calculations like [8] and experiments carried out in [9,10].

Recent experiments in the MICCA-Spray annular combustion chamber equipped with sixteen swirling injectors and powered by fuel spray revealed regimes with strong self-sustained combustion oscillations [10]. These instabilities were found to appear in the form of periodic bursts coupled to the first azimuthal 1A1L mode of the combustion chamber with acoustic pressure levels up to 5% of the chamber static pressure. The frequency of these instabilities was also shown to feature an intriguing pattern with large variations between 700 and 800 Hz during their growth and decay. One motivation of the present study is to gather data on the Flame Describing Function (FDF) of a single spray injector of the MICCA-Spray chamber to help unravel this complex dynamics.

In many theoretical analysis of combustion instabilities coupled to azimuthal modes [11–13], the flame response is modeled by a relationship linking the heat release rate oscillations $\dot{Q}'$ directly to pressure oscillations p' in the chamber. The modeling effort carried out in parallel has emphasized the fundamental role of the flame response to mass flowrate perturbations and a large number of studies have focused on the determination of Flame Transfer Functions (FTF) linking heat release rate fluctuations in the flame to incoming flow-rate disturbances [14–17]. The case of swirling flames of considerable technical interest was considered more recently [18,19]. An extension of the transfer function concept in the form of the Flame Describing Function (FDF) framework was developed to account for nonlinearities by representing the flame response in terms of frequency and amplitude of the impinging perturbation [20,21].

$$\mathcal{F}(\omega, u') = \frac{\dot{Q}'/\overline{\dot{Q}'}}{u'/\overline{u}} = G(\omega, u')\, e^{i\varphi(\omega,u')} \tag{1}$$

This nonlinear framework was successfully applied to determine the oscillation frequencies and oscillation levels of unstable modes in a premixed swirling combustor equipped with a single injector [19]. Analysis of the flame response to forced flow disturbances indicates that the flame shape defines to a large extent its linear [22] and nonlinear [23] dynamical response.

Many of the available investigations concern premixed flames while practical systems are often fed with liquid fuel. The later injection systems are also prone to thermo-acoustic instabilities [24–29]. A few studies report characterizations of the limit-cycle oscillations with OH* or CH* chemiluminescence measurements correlated with the spray dynamics [30,27,28]. In most cases there is a sizable pressure drop in the liquid fuel feed line providing a large impedance to impinging pressure perturbations so that one only needs to consider fluctuations in the air feeding manifold and injection unit. Laboratory scale experiments reported in the literature explore the sensitivity of the flame to these air flow rate modulations but are limited to just a few forcing frequencies at fixed amplitudes [31,24,25].

The acoustic response and FDF of swirling spray flames to a broad frequency range of air modulation was recently considered in [29] where the spray flames investigated feature a distinct response compared to those obtained for premixed swirling flames. In particular, the low frequency limit of the FDF gain differs from that found in the premixed case and tends to zero in that limit. The FDF phase lag was also found to depend on the perturbation level, a feature already observed in partially premixed systems [32]. Measurements in [29] were carried out in the case of steam assisted liquid fuel injectors. This short review of the literature indicates that the dynamical response of spray flames and more specifically swirling spray flames is not well documented. The present study tries to reduce this lack of knowledge.

The next section briefly describes the experimental set up (section 2). The acoustic response to external modulations is discussed in section 3. The system features natural, self-excited instabilities that are characterized in section 4. The forcing of the flame is compared to the self-excited case (section 5) to validate the methodology. The response of swirling spray flames is then examined using the FDF framework for nonlinear combustion instability analysis (section 6). The frequency response of the flame to acoustic perturbations is characterized by comparing the chemiluminescence signal generated by combustion and assumed to represent the heat release rate in the flame to the velocity signal measured upstream the injector. The present investigation aims at identifying parameters that control the sensitivity of spray flames to incident velocity perturbations. It is also indicated that the knowledge obtained and theoretical results can be used to predict the behavior of such injection systems when they are placed in an annular configuration.

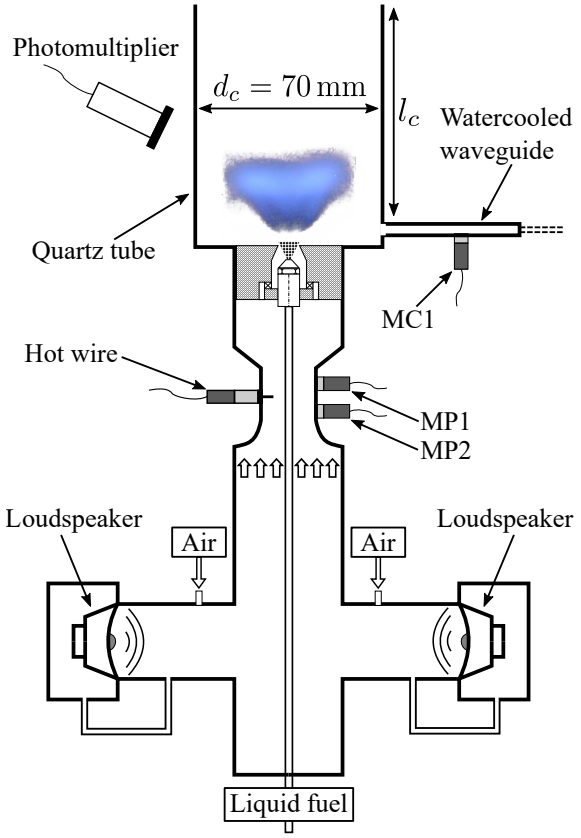

Fig. 1 Schematic of the SICCA-Spray burner to characterize flame dynamics with FDF measurements.

2 Experimental configuration

The experimental configuration represented schematically in Figure 1 comprises a plenum and a combustion chamber. The chamber is formed by a cylindrical quartz tube with a diameter $d_c = 70\,\text{mm}$ and of variable length l_c. Two driver units are plugged on the 300 mm cylindrical plenum to modulate the air flow. A swirled injection unit links the plenum to the combustion chamber. The injector is composed of an air circuit passing through a swirler and of a liquid atomizer to feed liquid fuel and form spray of droplets.

Air is injected at ambient temperature at the bottom of the plenum. It then reaches the injector where it passes through a radial swirler with six 4.5 mm holes and exits the injector with a measured swirl number of 0.63. The head loss through the injector is of the order of 4% of the atmospheric pressure at the nominal operating conditions investigated. Fuel (n-heptane) is injected using a simplex atomizer supplied pressurized at 9 bar. The atomizer generates a hollow cone and is positioned in the middle of the swirler. The droplet spray formed by this system has a mean diameter $d_{10} = 8\,\mu\text{m}$ and a SMD $d_{32} = 25\,\mu\text{m}$. The injector is terminated by a convergent section. Nominal injection conditions, used throughout this article, are as follows. Air flow rate is fixed at $\dot{m}_{air} = 2.59\,\text{g}\,\text{s}^{-1}$ and fuel flow rate is $\dot{m}_{fuel} = 0.144\,\text{g}\,\text{s}^{-1}$. The global equivalence ratio is $\phi = 0.85$ and the global power $\mathcal{P} = 6.5\,\text{kW}$. The bulk velocity of the air at the exit of the injector is $U_b = 43\,\text{m}\,\text{s}^{-1}$. Figure 2 presents the Abel transform of the CH* chemiluminescence of the flame using a Princeton Instrument PiMax 4 intensified camera. The flame takes a well defined M-shape, slightly lifted 10 mm above the chamber backplane. Detailed characterizations of the spray and of the airflow with laser optical diagnostics can be found in [10].

The Flame Describing Functions (FDF) based on the velocity perturbation u' and on the acoustic pressure fluctuation p' in the chamber are respectively defined by :

$$\mathcal{F}(\omega, |u'|) = \frac{\dot{Q}'/\overline{\dot{Q}}}{u'/\overline{u}} \tag{2}$$

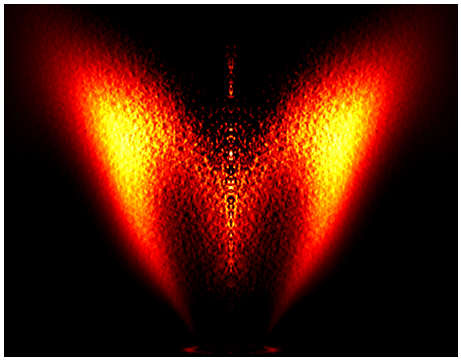

Fig. 2 Image in false colors of the Abel transform of the CH* chemiluminescence of the flame with $\phi = 0.85, \mathcal{P} = 6.5\,\mathrm{kW}, U_b = 43\,\mathrm{m\,s^{-1}}$. For symmetry, the Abel transform of one branch of the M-shape flame is deconvoluted using the Abel transform and replicated to generate the entire flame. The image is cropped in order to exhibit the exit of the burner on the bottom of the image.

$$\mathcal{F}(\omega, |p'|) = \frac{\dot{Q}'/\overline{\dot{Q}}}{p'/\bar{p}} \tag{3}$$

These two complex functions are measured with the diagnostics indicated in Figure 1. The gaseous flow is modulated by the two driver units of 150 W and 8 Ω each plugged in the plenum. Due to the relatively high head loss induced by the swirlers, these two units are enclosed in cavities linked to the plenum to balance the pressure on both sides of the driver unit membrane. The frequency of the oscillations ranges from 250 to 900 Hz. A sine-wave generator and an amplifier actuates the loudspeakers over this range. The amplitude u' of the perturbation generated in the upstream flow is determined using a hot wire placed 100 mm upstream the combustion chamber backplane. This region is chosen in order to have a nearly laminar velocity profile. Measured $u'/\overline{u}$ range from 0.1 to 1.3. Two microphones (MP1 and MP2) are placed around the same position to evaluate u' using a second method and check the hot wire measurements. A third microphone (MC1) measures the acoustic pressure p' in the chamber, pressure which appears in Eq. (3). It is flush mounted on a cooled waveguide directly plugged on the chamber backplane. A photomultiplier (PM) with an OH* filter is placed on the side of the combustion chamber to record the flame emission. The PM sensor is tilted towards the injector position in order to capture the entire flame luminosity whatever its shape. It is known that the OH* emission signal is proportional to the heat release rate in premixed flames. It is assumed in what follows and this is admittedly an approximation that there is a link between the two quantities in the present case where the flame is fed by a spray of droplets and it is considered that $I'/\overline{I} \simeq \dot{Q}'/\overline{\dot{Q}}$. It was shown in [29] that this approximation yielded reasonable results for instability predictions for globally lean injection conditions ($\phi < 1$).

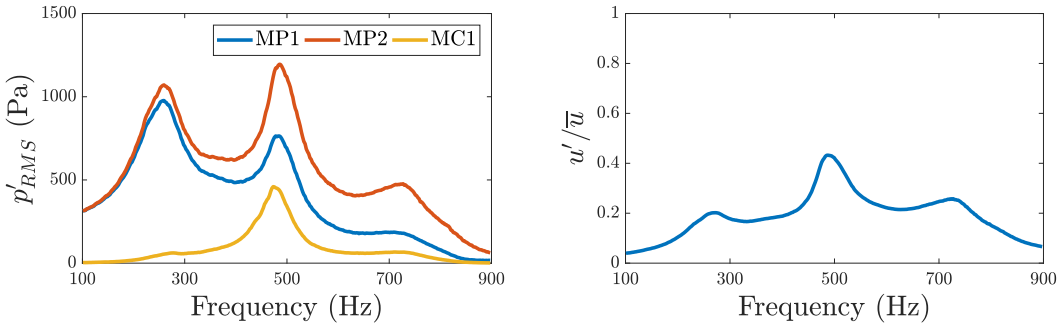

Fig. 3 Left: Acoustic response of the system for a range of frequencies up to 900 Hz under cold conditions with flowing air at $\dot{m}_{air} = 2.59\,\mathrm{g\,s^{-1}}$. The voltage of the excitation system is kept constant. Right: Measured velocity fluctuation ratio $u'/\overline{u}$ obtained with the hot wire.

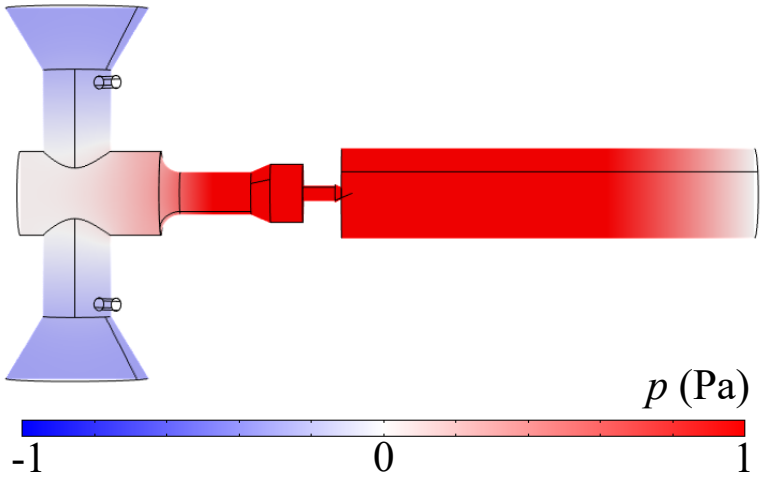

Fig. 4 Acoustic pressure p at 543 Hz calculated using a Helmholtz solver and assuming a constant temperature of 1200 K in the combustion chamber.

3 Frequency response of the system

In these first experiments there is no combustion and the system operates under cold flow conditions. The driver units are used to modulate the flow with increasing frequency from 100 to 900 Hz at a fixed voltage V_0 and the air flow is maintained constant at $\dot{m} = 2.59\,\mathrm{g\,s^{-1}}$. The resulting acoustic signals recorded using MP1, MP2 and MC1 are plotted in Figure 3, left. Two resonance peaks are found, one at 260 Hz and the other at 490 Hz. The first resonance corresponds to a pure plenum mode whereas the second is a coupled chamber-plenum mode. The right plot in Figure 3 shows the computed velocity fluctuation ratio $u'/\overline{u}$ with $\overline{u}$ the mean velocity, when the frequency f is increased at fixed voltage V_0. It is easy to see that $u'/\overline{u}$ is not constant over the frequency range. This is due to an acoustic resonance near 490 Hz increasing the velocity ratio and the nonlinear response of the loudspeaker. It is important to underline this feature as it will be the method used to evaluate the FDF in section 6.

A Helmholtz solver is used to calculate the mode shape in the system at the frequency of $f_h = 543$ Hz corresponding to one of the self-sustained combustion oscillation observed in the setup and analyzed in section 4 when the chamber length is varied. In this simulation, the temperature in the plenum is considered to be constant $T_1 = 300$ K while the temperature in the combustion chamber is $T_2 = 1200$ K. The length of the chamber is augmented to $l_{tot} = l_c + l_{end} = 320$ mm in the simulation with $l_c = 280$ mm the combustion chamber length and $l_{end} = 40$ mm the end-correction which has been measured (not shown here). For simplicity, the complex injector system has been replaced by an single hole of equivalent surface with the same length. Note that the convergent end-piece of the injector is taken into account in this simulation. The mode shape is shown in Figure 4 through a cut of the system. One can see that the mode is longitudinal, with a maximum pressure near the backplane. The cylindrical pipe where the hot wire is located (see Figure 1), has only a slightly lower amplitude level, but with the same sign.

4 Self-excited instabilities

For certain geometrical lengths l_c of the combustion chamber, the system exhibits well defined self-excited longitudinal instabilities. Frequency f, velocity fluctuation rate $u'/\overline{u}$, heat release rate $\dot{Q}'/\overline{\dot{Q}}$ ratios and acoustic level in the chamber p' are given in Table 1 for different lengths l_c. One finds that a critical chamber length is necessary to observe thermo-acoustic modes and, in the case of the SICCA-Spray burner, l_c needs to be greater than 245 mm to observe combustion instabilities. All self-excited instabilities are longitudinal modes developing in the chamber.

An example with $l_c = 280$ mm is now examined. Combustion instabilities appear in this case at 530 Hz. This frequency can be retrieved by considering a quarter-wave mode of the combustion

Table 1 Characterization of the self-excited instabilities as a function of the combustion chamber length l_c in the SICCA-Spray bench.

l_c (mm)	f (Hz)	$u'/\overline{u}$	$\dot{Q}'/\overline{\dot{Q}}$	p' (Pa)
215	595	0.06	0.01	19
230	605	0.08	0.07	175
245	565	0.36	0.34	1370
265	535	0.49	0.21	1170
280	530	0.38	0.16	890
295	455	0.63	0.28	1550
315	415	0.76	0.48	3020

chamber cavity. The mean temperature in the system is of the order of $T = 1200\,\mathrm{K}$ giving a speed of

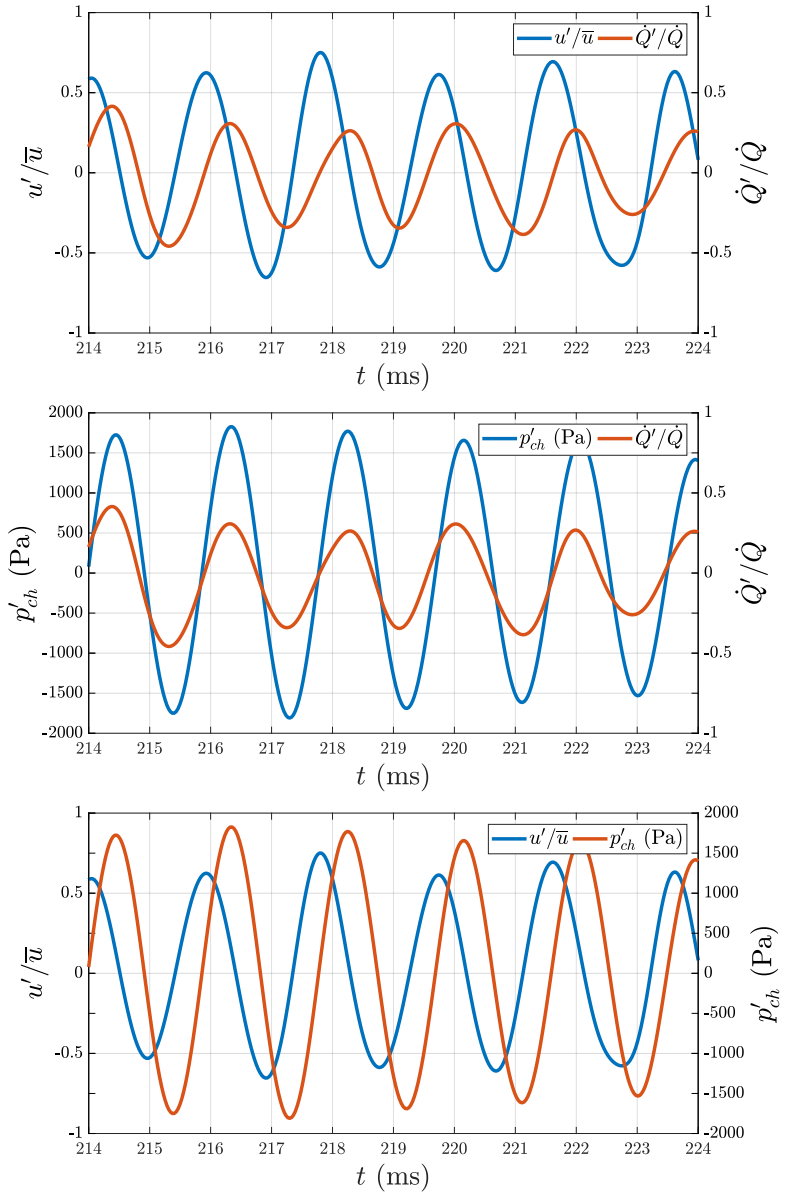

Fig. 5 Time series of velocity, acoustic pressure in the chamber and heat release rate fluctuations for the self-triggered flame with $l_c = 280\,\mathrm{mm}$. Data are normalized by their mean value except for the acoustic pressure. Signals are low pass filtered with a cut-off frequency f_c =1000 Hz.

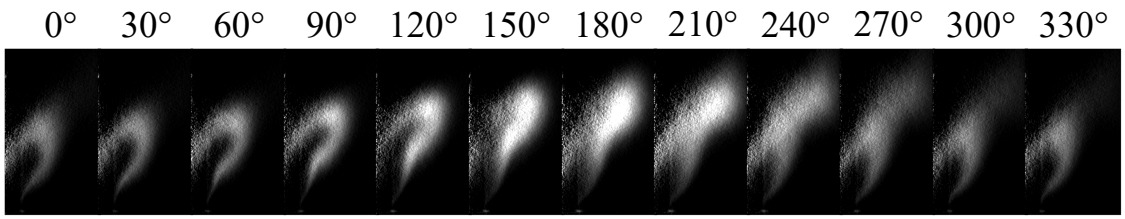

Fig. 6 Phased CH* chemiluminescence of the flame during one cycle of oscillation. Images are averaged over 600 cycles.

sound $c = \sqrt{\gamma r T} = 694\,\mathrm{m\,s^{-1}}$ in the medium. The natural resonant frequency is thus $f = c/4L = 540\,\mathrm{Hz}$ with $L = l_c + l_{end}$ and $l_{end} = 40\,\mathrm{mm}$ the measured end-correction. This calculation is confirmed by the Helmholtz analysis presented in Figure 4. Figure 5 presents the filtered velocity, acoustic pressure and heat release rate signals during the instability. The velocity fluctuations at the hot wire, in the top figure, are plotted along with the heat release rate fluctuations. One can see a clear sinusoidal response of the velocity with a fluctuation of $u'/\overline{u} = 0.5$ stable over the 2 s of recording. The heat release rate oscillates at the same frequency and with a phase φ_{uQ} of $\pi/2$ between the velocity and the heat release signals. The heat release ratio $\dot{Q}'/\overline{\dot{Q}}$ fluctuates around 0.25 while the acoustic pressure in the chamber p'_{ch} reaches a peak value of 1700 Pa. Acoustic pressure and heat release rate are oscillating perfectly in phase, at the same frequency, indicating that the Rayleigh criterion is satisfied. This implies that p'_{ch} and u' at the injector outlet are in phase quadrature because $i\rho\omega = \nabla p$. Note that the velocity u' which is plotted in Figure 5 is measured by the hot wire 100 mm upstream the combustion zone, where $\dot{Q}$ is measured by the photomultiplier. Between these two points, the information may not always travel at the acoustic velocity $c \sim 340\,\mathrm{m\,s^{-1}}$ all the way. It is known for example from [19] that the swirler induces a vorticity mode that propagates at the flow velocity in the injector unit. One may have to consider the energy transfer from the acoustic to the convective propagation mode which would indicate a major shift in the propagation velocity. LES calculations, not presented here, have demonstrated that the velocity perturbation u' is transported at the acoustic speed for approximately 80 mm, corresponding to the beginning of the injector unit in the system. The velocity then evolves in a complex manner in the injector.

Phased chemiluminescence images are recorded using a PiMax 4 camera equipped with a CH* filter. Images are then Abel transformed to retrieve the contribution of a slice to the flame emission. As the flame is axisymmetric, only half images of the right part of the flame are shown in Figure 6 corresponding to phases from 0 to 330°. One may note the strong flame displacement in the axial direction and a flame brush curving during the peak of the cycle around 180°. The flame length is also notably affected. The luminosity of the flame varies along its length. Note that the algorithm used to extract the flame slice allows a quantitative comparison of luminosity between the different images. The anchoring point of the flame is essentially fixed in space at a distance of 10 mm from the injector exhaust.

5 Forced flame response

In this section, the combustion chamber is equipped with a shorter flame tube $l_c = 165\,\mathrm{mm}$ to avoid self-excitation of instabilities. As in section 4, the dynamics of the flame is recorded using a photomultiplier and three microphones. Loudspeakers depicted in Figure 1 are actuated by a function generator and an amplifier to force the flame motion at a chosen frequency. The amplitude is modulated in order to get the desired velocity fluctuation rate $u'/\overline{u}$ at the hot wire location.

In Figure 7, the flame is forced at $f = 530\,\mathrm{Hz}$ and at an amplitude $u'/\overline{u} = 0.45$ to match the conditions corresponding to the self-excited instability with the l_c=280 mm flame tube. Velocity fluctuations are sinusoidal and at the same frequency and with a difference in amplitude of 10% in order to match with the self-excited case. The heat release rate fluctuations $\dot{Q}'/\overline{\dot{Q}}$ in the modulated case are nearly the same as those recorded in the naturally excited case. The main difference is found in the phase $\varphi_{uQ} = -\pi/2$ between velocity fluctuations and heat release rate fluctuations

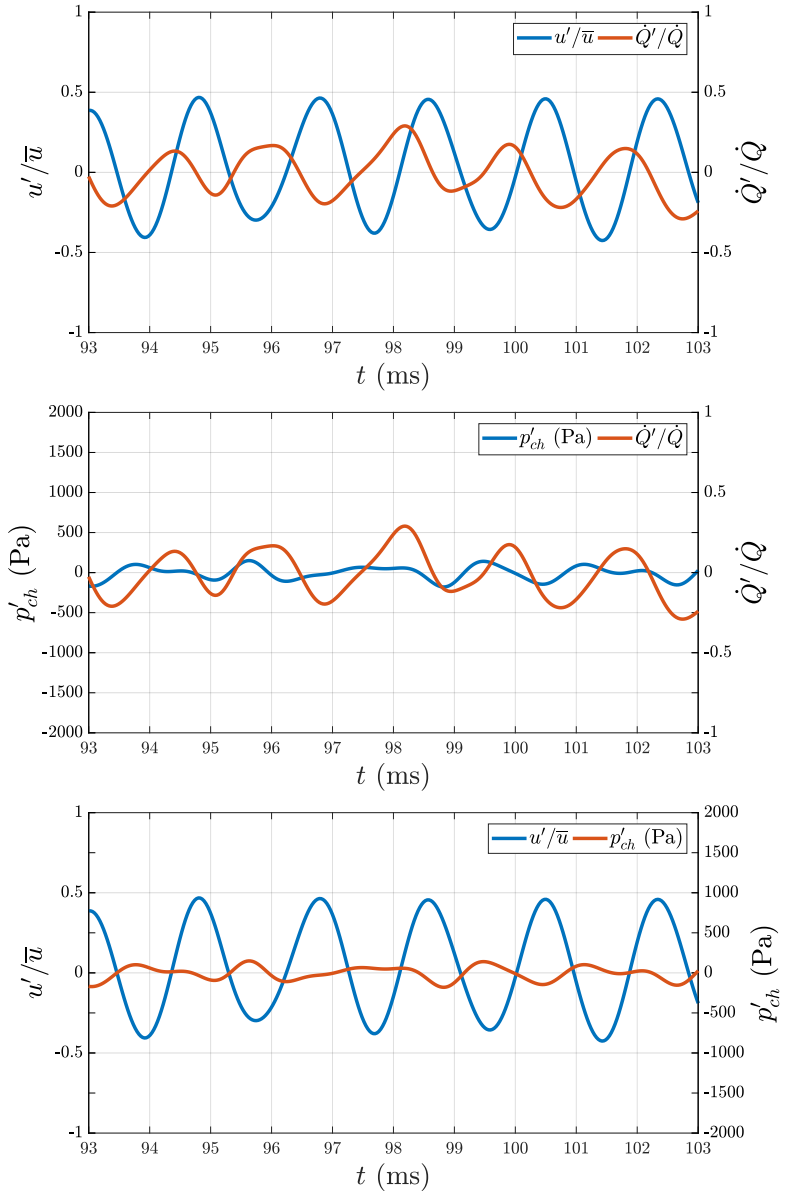

Fig. 7 Time series of velocity, acoustic pressure in the chamber and heat release rate fluctuations for the forced flame at 530 Hz. Data are normalized by their mean quantity except for the acoustic pressure. Signals are filtered with a low-pass filter at 1000 Hz.

which is the opposite of that found in the self-excited case. The second difference is in the acoustic pressure in the combustion chamber p'_{ch} which is much lower in the forced case. The pressure is around 200 Pa peak whereas the pressure in the self-excited flame is around 2000 Pa. This is the consequence of the length of the combustion chamber cavity (165 mm) that is not scaled to resonate at this frequency. Considering, as in the last section, the quarter-wave mode of the 165 mm tube, the resonant frequency is 850 Hz which is much higher then the excitation at 530 Hz. Thus the acoustic level is not amplified by the system resonance. This is an important result as many theoretical models take p' as an input to deduce $\dot{Q}'$. The present experiment shows that, in the case of a forced flame, p' is not an input but a result of $\dot{Q}'$. An alternative is to consider that $p' \sim d\dot{Q}/dt$ as for flames radiating noise in the free field, implying in this case a phase quadrature between the signals. These models might help to shed light on certain phenomena but they will always face the problem of their experimental validation. It is then more natural to take u' as the input of $\dot{Q}'$ but problems still rise as seen here. Where $\varphi_{uQ} = \pi/2$ when the flame naturally oscillates, $\varphi_{uQ} = -\pi/2$ when the flame is forced. This is the consequence of the velocity measurement method,

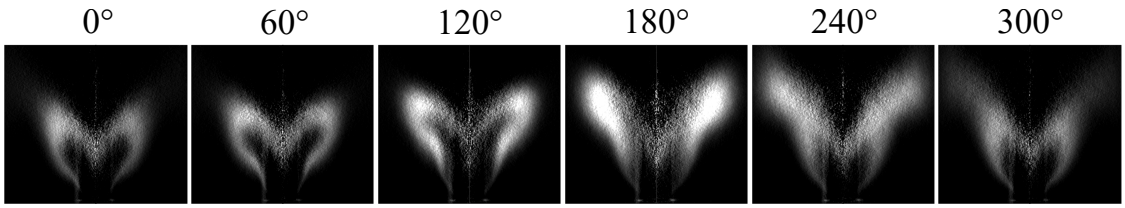

Fig. 8 Phased average CH* chemiluminescence of the flame during one cycle of oscillation for the forced flames (left branch of the flame) and for the self-triggered flames (right branch of the flame). Images are averaged over 600 cycles.

as mentioned before. These observations will be examined in section 6 when looking at different Flame Describing Functions. It is worth noting that numerical results using LES exhibits the same behavior concerning the phase difference φ_{uQ} in the case of the self-excited flame or in the forced case. Results are not included here but should be presented in another article.

CH* chemiluminescence images for the forced case are now compared with the images corresponding to the self-excited case. In Figure 8, the forced case is on the left hand side of each image while the self-excited case is on the right hand side. One can identify similar shapes in the flame motion as described before. The luminosity, the flame brush and the anchoring point vary in the same fashion.

In conclusion, the previous data indicate that the flame dynamics under external forcing and under self-excited oscillations at one particular frequency have similar characteristics. The flame shapes at different phases during the cycle are the same and the relative velocity and heat release rate levels have the same amplitude levels but the phase difference φ_{uQ} between velocity and heat release rate in the forced and in the self-excited case do not match. It is $+\pi/2$ in the first case and $-\pi/2$ in the second and this difference needs to be interpreted.

6 Flame Describing Function measurement

In this section, the Flame Describing Fuction (FDF) of the spray flame is evaluated using the SICCA-Spray burner shown in Figure 1. As described in section 3, if the frequency is increased with the voltage of the driver units kept constant, the resulting $u'/\overline{u}$ is not constant. A two-microphone method is also used to avoid signal aliasing when the velocity fluctuations become large enough to induce a bias in the hot wire measurements. Microphones MP1 and MP2 in the plenum are used to reconstruct the acoustic field. They are spaced by a distance $\Delta x = 50\,\mathrm{mm}$ and placed on the sides of the hot wire (see Figure 1). The velocity fluctuation u' at the hot wire point can be deduced from the following equation:

$$u' = \frac{1}{i\rho_0\omega}\frac{p'_2 - p'_1}{\Delta x} \tag{4}$$

where p'_2 and p'_1 are measured by microphones MP2 and MP1 respectively. The air density is taken $\rho_0 = 1.2\,\mathrm{kg/m^3}$ and $\omega = 2\pi f$ denotes the angular frequency. This method has been validated on the bench for several conditions (not shown here). Calculated u' values with Eq. (4) will then be used in the rest of this article for consistency. To obtain an FDF, one has then to sweep the excitation frequency from $f_1 = 100\,\mathrm{Hz}$ to $f_2 = 900\,\mathrm{Hz}$ for several output voltages V_0 of the function generator. Frequencies lower than 100 Hz are not explored for several reasons. First, the excitation system using loudspeakers has a low efficiency at frequencies under 200 Hz, making so that high amplitudes perturbations are difficult to reach. Secondly, the frequencies of interest are in the higher spectral range, around 500 Hz for both the single burner SICCA-Spray and the annular combustor MICCA-Spray.

A frequency ramp from f_1 to f_2 at a constant rate of $1\,\mathrm{Hz\,s^{-1}}$ is then used to modulate the system. Signals are recorded at a sampling frequency $f_s = 32{,}768\,\mathrm{Hz}$ during 2 s, ensuring that the forcing signal frequency only increases by 2 Hz and is essentially constant during the acquisition time. The transfer function is then estimated using the Welch's averaged periodogram method to calculate the Cross-Power Spectral Density (CPSD). The 2 s signals are divided into eight segments

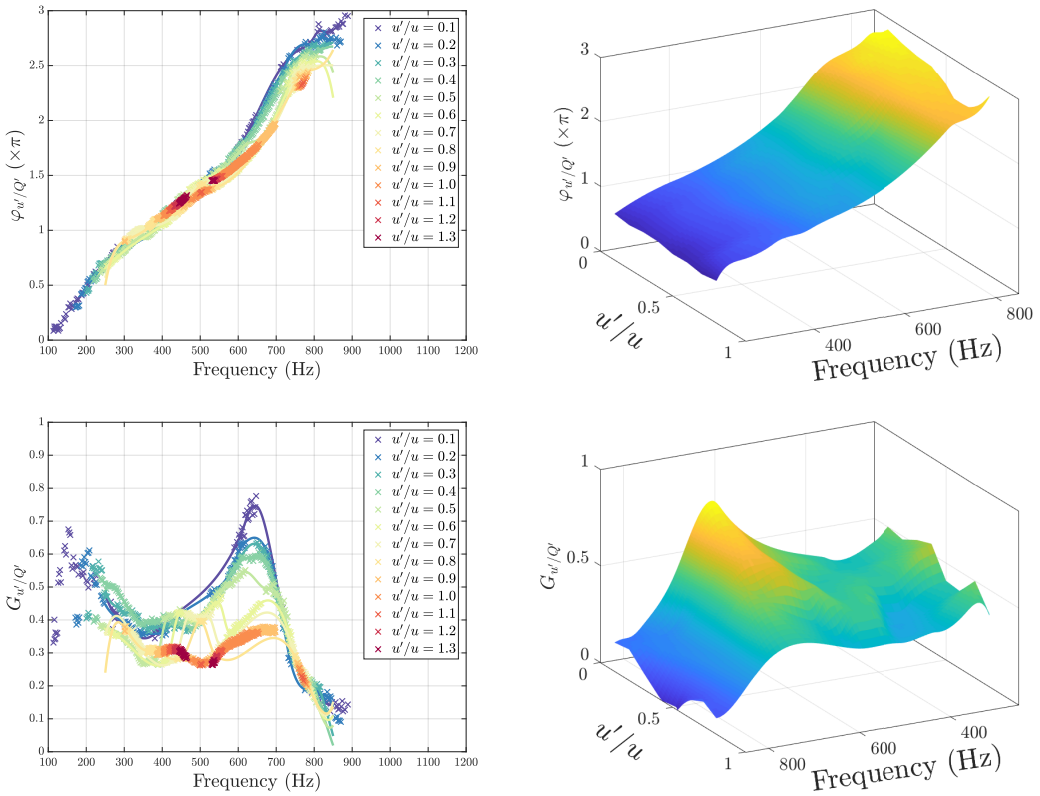

Fig. 9 FDF based on the velocity u' and the heat release rate $\dot{Q}'$. Left: Phase φ and gain G of the FDF between the velocity and the heat release rate ratio and their fit. Right: Linear interpolation of the FDF between $u'/\overline{u} = 0.1$ and 0.9 based on the results presented in the left hand side. Note that the frequency axis of the two figures are inverted.

with Hamming windows and a 50% overlap. The gain $G(f)$ and phase $\varphi(f)$ of the transfer function are then deduced at the modulation frequency f. This processing is done to evaluate the transfer functions between $u'/\overline{u}$ and $\dot{Q}'/\overline{\dot{Q}}$ and $p'/\overline{p}$ and $\dot{Q}'/\overline{\dot{Q}}$. This gives a large dataset of Flame Transfer Functions for different $u'/\overline{u}$ between f_1 and f_2. Data are finally processed to only keep specific values for $u'/\overline{u}$ ranging from 0.1 to 1.3 with a spacing of 0.1. For each $u'/\overline{u}$ value, a 5% error in the estimation of the velocity fluctuation ratio is admitted. Data are then interpolated for $u'/\overline{u} < 0.9$.

The FDF based on the velocity $u'/\overline{u}$ and the heat release rate $\dot{Q}'/\overline{\dot{Q}}$ ratios is displayed in Figure 9. The left figures represent 2D-plots of phase (top) and gain (bottom). Data are fitted for $u'/\overline{u}$ up to 0.8. This value is limited on purpose because higher values cannot be applied in various frequency ranges due to the difficulty to excite high levels of fluctuations over a wide range of frequencies. On the right hand side, a linear interpolation is applied to $u'/\overline{u}$ to give a better understanding of the flame response. One observes that the phase increases quasi linearly across the frequency range. The impact of the velocity ratio $u'/\overline{u}$ ratio is small except in the band 600 700 Hz where one can find a difference of 1 rad between the FDF phase lags for $u'/\overline{u} = 0.1$ and 0.8. Based on the phase φ, the time lag $\tau = \phi/(2\pi f)$ can be estimated. Considering that the phase slope is rather constant across the frequency range, $\tau = 1.8$ ms.

In the gain plot (bottom left), the amplitudes at low frequencies are scattered. The trend in gain is clearer when the frequency reaches 300 Hz. One can then observe a peak at 640 Hz. Note that this value is far from the natural resonant frequency of the system, indicating that this is the result of the flame response. The gain strongly decreases when $u'/\overline{u}$ is increased, demonstrating the nonlinearity of the phenomenon and the saturation of the flame response at high amplitudes of modulation.

Theory provides possible bands of instability. These bands plotted in gray in the following phase diagrams are approximately bounded by horizontal lines corresponding to $\{\pi, 2\pi\}$. When

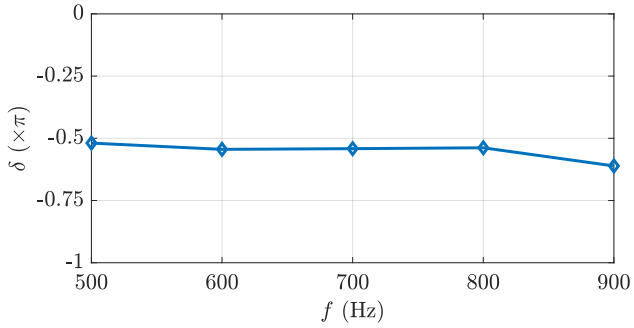

Fig. 10 Evaluation of the phase of the injector admittance δ for frequencies between 500 and 900 Hz.

$\pi < \varphi < 2\pi$ [mod. 2π], the configuration is potentially unstable, a result already reported in [17, 33,34]. This first consideration does not take into account the possible role of the injector on the stability. The admittance of the injector has to be considered because the velocity measurement, made with the hot wire, is carried out on the upstream side of the injector. Thus the measured transfer function is not only linked to the flame contribution but also to the impact of the injector. To include this admittance, one has to shift the phase of the FDF by the value measured in Figure 10. It is now possible to estimate the bands of instability of the system by analysing the phase diagram with the following expression:

$$\pi < \varphi + \delta < 2\pi \ \ [\text{mod}.2\pi] \tag{5}$$

with the flame contribution to the instability between $\{\pi, 2\pi\}$ and the injector admittance δ, shifting the phase. To estimate δ, a velocity perturbation at variable frequency is applied to the system using the excitation system under cold conditions. The velocity fluctuation is first measured with the hot wire and, during another experiment, with a Laser Doppler Anemometry (LDA)

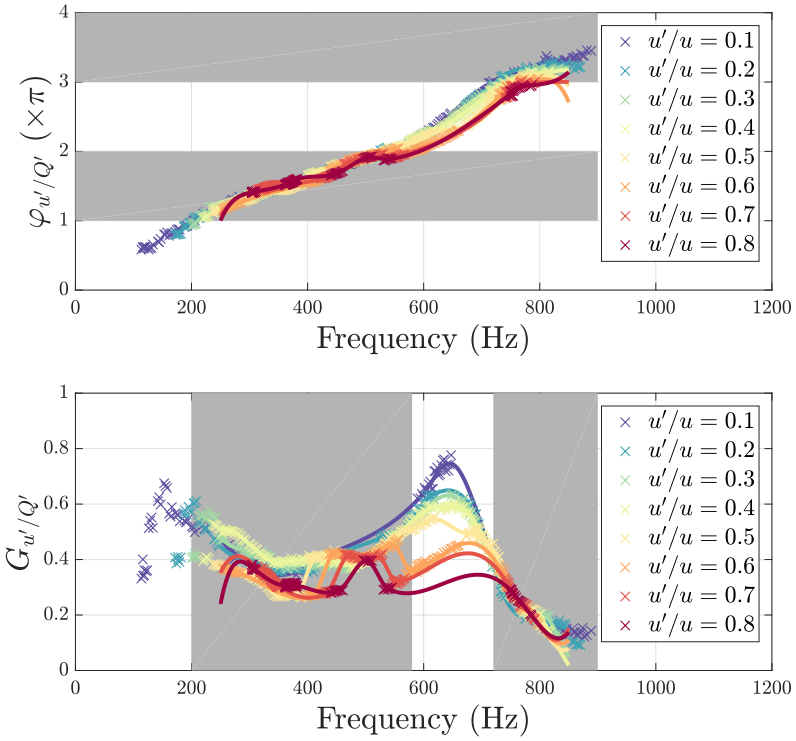

Fig. 11 Top: Phase φ of the FDF and burner admittance coupled with the instability band in grey. Bottom: Gain G with the deduce position of the instability bands.

system at the exit of the burner, in the air jet. The phase between the velocity fluctuation u' and the reference signal from the function generator is calculated in both cases. One can then deduce the phase between the velocity fluctuation at the hot wire and at the exit of the burner. The measurement of δ is presented in Figure 10 for several frequencies. One can see that it is quite constant with the frequency and may be considered to be close to $-\pi/2$. Figure 11, top, shows the position of the two instability bands in grey. It is then possible to calculate the frequency boundaries of the potential unstable modes. One can see that the phase enters the first instability band around 200 Hz and up to 580 Hz for the highest levels of $u'/\overline{u}$. It enters the second band at 720 Hz until the end of the FDF estimation at 900 Hz. This explains why the SICCA-Spray bench exhibits powerful naturally excited instabilities when the different length l_c of the walls is increased. When the resonant frequency of the system becomes lower than 550 Hz, the system is potentially unstable. The more the resonant frequency decreases, the more the system becomes unstable. This is confirmed by the increase in $\dot{Q}'/\overline{\dot{Q}}$ observed in Table 1 when l_c increases. Note that the forced flame with $l_c = 165$ mm is not naturally unstable. As indicated before, the resonant frequency would be 850 Hz. This value is in a potential unstable band but the gain is very low in this region with $G < 0.08$, probably much lower than the damping of the system.

One may infer from the previous considerations the stability or instability of a combustion chamber equipped with multiple swirl spray injectors. Considering an annular combustor like the MICCA-Spray system investigated at EM2C lab where the fundamental frequency of the first azimuthal mode (1A1L) is around 750 Hz (experiments and a modal analysis are available in [10]).

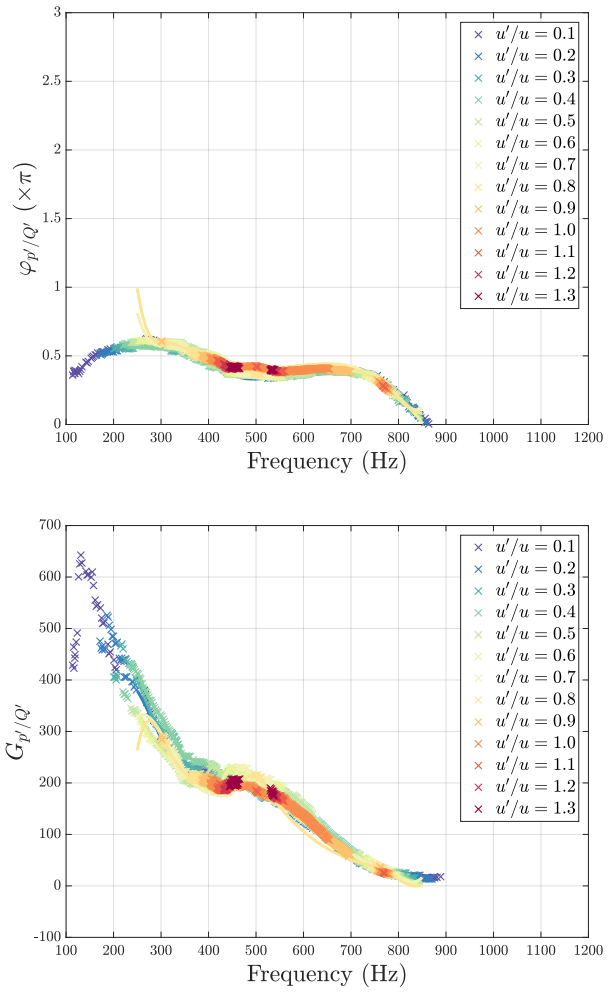

Fig. 12 FDF based on the acoustic pressure in the chamber p' and the heat release rate $\dot{Q}'$. Top: Phase φ and gain G of the FDF for the velocity and the heat release rate ratio and their fit.

The instability intervals in Figure 11 contains the eigenfrequency $f = 750\,\text{Hz}$ of the 1A1L mode. One may note however that this criterion is not sufficient to ensure that the system will be linearly unstable. This will be the case if the growth rate at low amplitude is greater than the damping rate. For this to be the case, the gain of the FDF must be sufficiently large, but one also notices that this gain is relatively low at the frequency of the 1A1L mode ($G < 0.4$). An issue that is not considered in the previous analysis is that of the possible influence of mutual interactions between adjacent flames and that of a suitable representation of the thermal conditions of the annular combustor. One then can expect that interactions between flames might modify the FDF determined on a single burner, but this is not yet quantified.

Note that the SICCA-Spray bench is equipped with a pressure sensor in the chamber (MC1), giving access to the acoustic pressure p' at the flame base during the forcing of the flame. This can be used to determine an FDF based on the pressure p' and on the heat release rate $\dot{Q}'$ as shown in Figure 12. The behavior of this FDF is quite different from that of the standard FDF based on the velocity u'. The phase does not evolve in a linear fashion with increasing frequency, it is nearly equal to $\pi/2$ over most of the frequency range. The measured p'_{ch} corresponds to the combustion noise induced by the flame in the combustion chamber. This radiated noise is in phase quadrature with the heat release rate fluctuation because $p'_{ch} \propto d\dot{Q}'/dt$ [35,36]. The gain has also a different shape as it decreases with frequency. No peak can be detected but there is a small bump around 450 Hz probably due to a coupling with a resonant mode of the system (see Figure 3). One may note that the gain and the phase barely change when the forcing amplitude is increased. These measurements confirm the observations made on the forced case in section 5 where it has been seen that the acoustic pressure in the chamber p' has a low amplitude that is not representative of the self-excited flame. The conclusion on the phase φ_{pQ} also holds as it is constant over most of the frequency range of the FDF.

7 Conclusion

This article is concerned with the determination of the Flame Describing Functions of swirling spray flames. These functions are obtained by making use of a single injector combustion system comprising a set of driver units. The system is used in two modes, the first of which corresponds to external modulation while the second pertains to self-excited oscillations. FDFs are determined in the first mode and the flame dynamics is observed using phase average imaging. In the second mode, the oscillation corresponds to a resonance of the system and is coupled by a longitudinal acoustic mode of the system involving the plenum and the combustion chamber. It is then possible to compare the flame response under external modulation to the response observed when the system is self-excited. Potential bands of instability are inferred from an examination of the measured FDF phase response measured in this single injector configuration and the possibility of instability in the MICCA-Spray annular system is deduced from these data. Finally, the FDF measured considering the acoustic pressure radiated by the flame in the chamber is investigated. It is shown that this quantity is not a proper input for the FDF as it does not provide a suitable portray of the of the dynamics of the combustion region. In effect the measured pressure is more of an output of the unsteady flame and cannot be taken as an input. This illustrates the difficulty of experimental determinations of relations linking the heat release rate fluctions to the pressure signal. It is finally shown that the classical FDF linking the heat release rate to the velocity fluctuation can be used effectively to predict instability trends of the single injector system and to predict possible unstable operation of the MICCA-Spray annular combustor.

Acknowledgements This work was supported by Safran Tech and by CNRS. The authors wish to thank J. Beaunier, Y. Le Teno and E. Jean-Bart for the technical support provided to this research.

References

1. U. Krüger, J. Hüren, S. Hoffmann, W. Krebs, D. Bohn, in *Proceedings of ASME Turbo Expo 1999, Paper 99-GT-111* (1999), 99-GT, p. 111
2. B. Schuermans, W. Polifke, C.O. Paschereit, in *ASME Conference Proceedings Paper 99-GT-132* (1999)
3. W. Krebs, P. Flohr, B. Prade, S. Hoffmann, Combustion Science and Technology **174**(7), 99 (2002)

4. J.P. Moeck, M. Paul, C.O. Paschereit, in *ASME Conference Proceedings, Paper GT 2010-23577* (Asme, 2010), pp. 1219–1232
5. N.A. Worth, J.R. Dawson, Proceedings of the Combustion Institute **34**(2), 3127 (2013)
6. N.A. Worth, J.R. Dawson, Combustion and Flame **160**(11), 2476 (2013)
7. J.F. Bourgouin, D. Durox, J.P. Moeck, T. Schuller, S. Candel, in *Proceedings of ASME Turbo Expo 2013* (San Antonio, Texas, USA, 2013), GT2013-95010
8. M. Boileau, G. Staffelbach, B. Cuenot, T. Poinsot, C. Berat, Combust. Flame **154**, 2 (2008)
9. K. Prieur, D. Durox, J. Beaunier, T. Schuller, S. Candel, Proceedings of the Combustion Institute **36**(3), 3717 (2017)
10. K. Prieur, D. Durox, J. Beaunier, T. Schuller, S. Candel, Proceedings of the Combustion Institute **36**(3), 3717 (2017)
11. B. Schuermans, C.O. Paschereit, P. Monkewitz, in *44th AIAA Aerospace Sciences Meeting and Exhibit* (2006), 2006-0549
12. N. Noiray, B. Schuermans, Proceedings of the Royal Society A: Mathematical, Physical and Engineering Science **469**(20120535 (15 pages)) (2013)
13. G. Ghirardo, M. Juniper, J.P. Moeck, Journal of Fluid Mechanics **805**, 52 (2016)
14. A. Dowling, Journal of Fluid Mechanics **394**, 51 (1999)
15. S. Ducruix, D. Durox, S. Candel, Proceedings of the Combustion Institute **28**(1), 765 (2000)
16. S. Candel, Proceedings of the Combustion Institute **29**, 1 (2002)
17. T. Schuller, D. Durox, S. Candel, Combustion and Flame **134**, 21 (2003)
18. G. Borghesi, F. Biagioli, B. Schuermans, Combustion theory and modeling **13**(3), 487 (2009)
19. P. Palies, D. Durox, T. Schuller, S. Candel, Combustion and Flame **158**(7), 1980 (2011)
20. A.P. Dowling, Journal of Fluid Mechanics **346**, 271 (1997)
21. N. Noiray, D. Durox, T. Schuller, S. Candel, Journal of Fluid Mechanics **615**, 139 (2008)
22. K.T. Kim, J.G. Lee, B.D. Quay, D.A. Santavicca, Combustion and Flame **157**, 1731 (2010)
23. D. Durox, T. Schuller, N. Noiray, S. Candel, Proceedings of the Combustion Institute **32**(1), 1391 (2009)
24. F. Giuliani, P. Gajan, O. Diers, M. Ledoux, Proceedings of the Combustion Institute **29**, 91 (2002)
25. P. Gajan, A. Strzelecki, B. Platet, R. Lecourt, F. Giuliani, Journal of Propulsion and Power **23**(2), 390 (2007)
26. T. Yi, D.A. Santavica, Journal of Propulsion and Power **25**(6), 1259 (2009)
27. T. Yi, D.A. Santavicca, Journal of Propulsion and Power **28**(5), 1000 (2012)
28. T. Providakis, L. Zimmer, P. Scouflaire, S. Ducruix, Journal of Engineering for Gas Turbines and Power **134**(11), 111503 (2012). DOI 10.1115/1.4007200
29. C. Mirat, D. Durox, T. Schuller, Proceedings of the Combustion Institute **35**(3), 3291 (2015)
30. J. Eckstein, E. Freitag, C. Hirsch, T. Sattelmayer, Journal of Engineering for Gas Turbines and Power **128**(April 2006), 264 (2006)
31. E. Haile, O. Delabroy, F. Lacas, D. Veynante, S. Candel, Symposium (International) on Combustion **26**(1), 1663 (1996)
32. K.T. Kim, S. Hochgreb, Combustion and Flame **158**, 2482 (2011)
33. D. Durox, T. Schuller, N. Noiray, A.L. Birbaud, S. Candel, Combustion and Flame **156**(1), 106 (2009)
34. D. Durox, J.P. Moeck, J.F. Bourgouin, P. Morenton, M. Viallon, T. Schuller, S. Candel, Combustion and Flame **160**(9), 1729 (2013)
35. I.R. Hurle, R.B. Price, T.M. Sugden, a. Thomas, T.M. Sudgen, a. Thomas, Proc. Roy. Soc. A **303**(1475), 409 (1968). DOI 10.1098/rspa.1968.0058
36. T. Schuller, D. Durox, S. Candel, Combustion and Flame **128**(1-2), 88 (2002). DOI 10.1016/S0010-2180(01)00334-0